AIMS Mathematics, 10(8): 17894–17921.
DOI: 10.3934/math.2025797
Received: 15 May 2025
Revised: 08 July 2025
Accepted: 15 July 2025
Published: 07 August 2025

https://www.aimspress.com/journal/Math

Research article

Exploring the dynamics of bacterial growth in oral biofilm causing dental caries: A study of deterministic modeling

Sanubari Tansah Tresna[1], Nursanti Anggriani[2,*], Herlina Napitupulu[2] and Wan Muhamad Amir W. Ahmad[3]

[1] Doctoral Program of Mathematics, Faculty of Mathematics and Natural Sciences, Universitas Padjadjaran, Indonesia
[2] Department of Mathematics, Faculty of Mathematics and Natural Sciences, Universitas Padjadjaran, Indonesia
[3] School of Dental Sciences, Universiti Sains Malaysia, Malaysia

* **Correspondence:** Email: nursanti.anggriani@unpad.ac.id.

Abstract: Dental caries is a health issue characterized by the attachment of an oral biofilm that contains bacteria to tooth surface. At present, several deterministic models have been constructed to explore numerous phenomena related to population dynamics. Despite the existing models, only two pieces of literature have explored bacterial growth in oral biofilms using ordinary differential equations with a deterministic modeling approach. Therefore, this study aims to propose a deterministic model to assess the dynamics of bacterial growth in oral biofilms, considering the interaction between the microorganisms. The model focuses on 3 bacteria, namely *Streptococcus mutans* (*S. mutans*), *Streptococcus sanguinis* (*S. sanguinis*), and *Veillonella spp*. A mathematical assessment was performed to ensure that the obtained solutions were feasible for biological discussion. Subsequently, the ratio of *S. mutans* against *S. sanguinis* under the equilibrium was formulated as the threshold to measure the risk level of caries formation. Additionally, a sensitivity analysis was also performed to appraise the parameters' influence on the observed dynamics. The results showed that there was a positive correlation between the presence of *Veillonella spp.* and an increased risk of caries formation. The theory of optimal control was used to investigate the optimal scenario for intervening in the threshold ratio by considering the effect of antibacterial utilization. Lastly, a numerical simulation was conducted to confirm the analysis results and scrutinize each bacterial dynamics under several scenarios represented by the selected parameter with varied values.

Keywords: bacterial growth; dental caries; deterministic modeling; dynamical system; numerical simulation; ordinary differential equations
Mathematics Subject Classification: 34A34, 37N25, 92C60

1. Introduction

Dental health issues are among the most significant global health challenges, affecting various people around the world. These issues not only affect the tooth and its gum but also cause various chronic diseases. According to the World Health Organization (WHO), approximately 3.5 billion people worldwide suffer dental health issues [1], with dental caries being the most prevalent (43%). Dental caries is a chronic disease that affects both oral and dental function [2]. Several studies have shown that it is the foremost cause of dental losses in children and adults and harms the dental roots of older people [3]. Therefore, it is essential to explore the cause, its progression, and the means to control the disease prevalence.

Dental caries causes damage to oral health and function and increases the prevalence of other chronic diseases. For example, a hole in the tooth can cause the bloodstream to open, which allows bacteria that live in the oral biofilm the chance to enter the bloodstream and travel to other parts of the body [4]. This is consistent with several studies that reported the presence of bacteria that cause dental caries in the lungs of pneumonia patients [5], the brain of dementia/Alzheimer patients [6], and the heart of endocarditis patients [7]. Therefore, the disease can be viewed as an early indicator, thus emphasizing the importance of an individual's health maintenance.

According to previous studies, dental caries is caused by an imbalance between tooth minerals and bacteria in oral biofilms [8]. Bacteria living in the oral cavity form colonies wrapped in an organic matrix with polysaccharides, proteins, and DNA from cell secretions to protect the microorganisms. The tooth surface is a part that is vulnerable to the attachment of bacterial colonies and their metabolic products [9]. The mechanism of dental caries is the accumulation of weak organic acids produced by *S. mutans* in biofilms due to the fermented carbohydrate metabolism [10]. These acids cause the local pH to fall below the threshold (pH <5.5), thereby facilitating the demineralization of the tooth tissue. The existence of *Veillonella spp*. supports the role of *S. mutans* in biofilm formation [11] and produces lactic acid that can damage the tooth enamel [12]. However, *Veillonella spp*. uses the acids produced by *S. mutans* as a source of carbon and energy, thus leading to the production of weaker acids [12,13] and a reduction in the risk of dental caries formation [14]. An overpopulation of *S. mutans* and *Veillonella spp*. in biofilms causes the severe demineralization of tooth tissue characterized by the diffusion of calcium, phosphate, and carbonate, as well as the formation of cavities [2].

An oral biofilm is a bacterial community that adheres to the tooth surface and significantly affects the quality of oral health. Dysbiosis in oral biofilms is defined as a condition when there is an increase in acid-producing and acid-fast bacteria, specifically *S. mutans* and Lactobacilli [15]. *S. mutans* is the bacteria most often discussed in dental caries studies [16]. Zhang et al. [17] and Zhu et al. [10] revealed that it often adhered to the tooth surface and plays a vital role in forming oral biofilms. *S. mutans* is often dominant in cariogenic areas [18] because it has better survival rates compared to other species, such as *S. sanguinis*, *S. oralis*, and *S. parasanguinis* [10]. An overpopulation of the microbe in oral biofilms causes an imbalance of the bacterial varieties and the occurrence of dental caries [19]. In addition, the discovery of *Veillonella spp*. in cases of dental caries has recently become one of the most

discussed topics. Setiawan et al. [20] revealed that the presence of *Veillonella spp*. is one of the factors in the occurrence of dental caries in children. Furthermore, Zhou et al. [13] stated that *Veillonella spp*. and *S. mutans* can be viewed as risk factors for the onset of the disease. However, Wicaksono et al. [14] reported that *Veillonella spp*. has the potential to neutralize the acid produced by *S. mutans* and inhibit the process of dental caries formation. This indicates that the growth and interaction between *S. mutans* and *Veillonella spp*. need to be studied for effective control and prevention.

Havsed et al. [21] reported that 3 main factors must be considered, namely socio-cultural, physiological, and dental (host). These factors do not necessarily require commensalism as the initial cause of dental caries. The influence of lifestyle has been reported to be an initial risk factor for tooth demineralization. For example, the consumption of carbohydrates that can differentiate into substrates supports the existence of bacteria in the oral cavity. *S. mutans* bacteria that exist in tooth production produce lactic acid, which degrades non-resistant microbes. Meanwhile, *S. mutans* is resistant to acidic conditions and can replicate, which leads to dysbiosis in dental plaque. In this condition, the pH level around the tooth decreases, which results in demineralization. Continuous demineralization often leads to the formation of cavities in the tooth.

The control of dental caries can be performed using 2 approaches, namely reducing the transmission risk of *S. mutans* bacteria between individuals and suppressing the existence of the bacterial population in oral biofilms. Control through educational interventions in the community can reduce the number of cases and the risk of oral biofilm formation [22]. In addition, Czajkowska et al. [23] explained that educational efforts can help individuals maintain dental and oral health and provide insight into early detection methods. Moreover, dental caries antigens or vaccines can also be considered to reduce the risk of oral biofilm formation [24,25]. Control through *S. mutans* transmission approach is typically performed by minimizing activities that allow the transfer of saliva between individuals [26], while the population growth approach uses antibiotics [3,27] and herbal ingredients [19].

Based on previous studies, deterministic modeling is frequently used to represent the growth of microorganisms and bacteria. This approach can assess and juxtapose a dynamic phenomenon under many scenarios as a case study to predict and formulate the needs of health policies [28]. Mathematical models help in quantitively perceiving the phenomenon and investigating whether the hypotheses fulfill the aims and goals of the study [29]. Constructing a model for the bacterial growth phenomenon requires assumptions about the growth and dynamic mechanisms influenced by either the environment or the existence of other bacteria. Several deterministic models have been introduced to investigate the bacterial dynamics for issues using various methods. Stanescu et al. [30] and Scott et al. [31] formulated a differential equation model to represent the bacterial dynamics by considering limited substrates and the nutrient quality that supports its growth. Later, Ibarguen et al. [32] developed a model that represented a resistant bacterium against multiple antibiotics and considered spontaneous mutations. Meanwhile, Cogan et al. [33] proposed a model that figured the persister bacterial dynamics by manipulating its killing time. Benjamin et al. [34] modeled the dynamics of bacteria by considering the pH variations of their environment and the use of bacteriocin synthesis. In terms of bacterial dynamics that cause a disease, Smith et al. [35], Cantone et al. [36], and Dominguez-Huttinger et al. [37] proposed a within-host model, which represents the dynamics that cause lung infections or pneumoniae from *Streptococcus pneumoniae*. Only two models have been proposed to study dental caries [38]. Shen et al. [39] constructed a complex bacterial dynamics model that was rooted in oral biofilms, but it did not consider the interaction among bacteria. Jing et al. [40] reconstructed the product [39] into a more

straightforward form, but did not explore bacterial interactions.

Based on the explanations above, it is essential to take advantage of a deterministic model to explore the dynamics of bacteria in oral biofilms by considering interventions and bacterial interactions is essential. To achieve the goal of suppressing the case of dental caries, a new model, distinct from those proposed by [39] and [40], was constructed and analyzed in this current study. In addition, a total of 3 types of bacteria were considered for assessment. First, the dynamics of *S. mutans* as the most dominant bacteria and most discussed in dental caries formation studies were assessed [21,25,41]. Additionally, *S. sanguinis* was also explored as a bacteria that can prevent caries formation by competing with the existence of *S. mutans* through the secretion of chemical compounds that can influence the acidity level around oral biofilms [25,27,42]. In addition, the existence of *Veillonella spp.* in the oral biofilms was evaluated [13,20,43,44] to mathematically identify its role in caries formation. The motive which underlies this study is to not only broaden the research scope of deterministic modeling but also to contribute theoretical and numerical insights to the dental community to minimize the potential caries cases. This is in line with the third Sustainable Development Goal and conceiving a caries-free Indonesia by 2030.

The remaining parts of this study is structured as follows. In the second section, the deterministic model formulation is presented by considering some assumptions obtained during the literature review. Next, the model is analyzed to ensure that the upcoming equilibrium solution fulfills the criterion of representing a biological entity. In the fourth section, sensitivity analyses are performed to show the most influential factor against the bacterial dynamics in oral biofilms. Subsequently, an optimal control model was proposed and analyzed in terms of attaining the Maximum Pontryagin Principle. The numerical simulation results are presented in the sixth section. Finally, the article ends with an essential conclusion by highlighting the results and elaborating on potential factors that have yet to be accommodated for further study.

2. Mathematical model

The model construction begins with determining the bacteria to be studied, which is based on information and data from literature reviews. *S. mutans* and *S. sanguinis* are the 2 most widely studied bacteria in the growth and development of biofilms, as well as the formation of dental caries [3,12,27,45]. *S. mutans* bacteria are known to produce organic acids due to the fermented carbohydrate metabolism in oral biofilms [14]. This acid causes the local pH to fall below the tolerance threshold of pH <5.5. Meanwhile, as a competitor bacterium, *S. sanguinis* does not have a good tolerance to acidic conditions. As a result, *S. mutans* tends to reproduce more efficiently, and the local pH can be lower. The local pH conditions can continuously decrease over a long period and cause demineralization, which leads to the formation cavities in the tooth. The presence of *S. sanguinis*, which produces hydrogen peroxide (H_2O_2), can disrupt the survival of *S. mutans* [46,47]. Mount et al. [48] revealed that the tendency for poor dietary patterns and an indifference to oral acidity conditions are supporting factors for the growth of *S. mutans*.

Veillonella spp. is another bacterium considered in this study. Several recent studies have shown the need to explore the role of *Veillonella spp.* in the formation of dental caries. Setiawan et al. [20] and Zhou et al. [13] revealed that *Veillonella spp.* were positively correlated with the growth of *S. mutans*. In this case, *Veillonella spp.* played a role in maintaining the pH acidity, and these did not reach extreme acidity conditions that interfered with the reproductive ability of *S. mutans* [49]. Bowen

et al. [12] explained that *Veillonella spp.* maintained the pH acidity, and it did not reach extreme conditions by breaking down the acid produced by *S. mutans* into weaker acids. In addition, *Veillonella spp.* can break down H_2O_2 into H_2O and O_2, which do not interfere with the survival of *S. mutans* [50,51]. Wicaksono et al. [14] explained that *Veillonella spp.* acted as an acid neutralizer that played a role in inhibiting tooth caries formation.

The formulation of a mathematical model of bacterial population dynamics in oral biofilms requires the following assumptions:

(1) The growth rate and natural death rate of each bacterium are constant.
(2) The carrying capacity is defined for each bacterium and is based on growth-supporting factors.
(3) The growth of *Veillonella spp*. bacteria is highly dependent on the existence of *S. mutans* and *S. sanguinis* bacteria.

The model considers antibacterial treatments with varying effects on each type of bacterium. This was done to gain insight into the benefits and risks of using antibacterials to control bacterial growth and prevent the formation of cavities in the tooth. Furthermore, exploring the influence of antibacterials can be used to measure the threshold of dental caries risk, which was represented by comparing the amount of *S. mutans* to *S. sanguinis* [52]. In this case, a smaller the ratio between *S. mutans* and *S. sanguinis* population indicated the lower the risk of caries formation.

The population dynamics model for each bacterium is described as follows:

(1) *S. sanguinis* population notated by S.

This population is influenced by constant natural growth and death rates, which are denoted as Λ_1 and μ_1, respectively. Nevertheless, according to the limited growth-supporting factors, the carrying capacity for *S. sanguinis* is involved and denoted as K_s. In addition, the *S. sanguinis* population can decrease due to the influence of local acidity, which implies acidic compounds released by *S. mutans*. In this case, the rate of this phenomenon is denoted as ζ_1. The role of *Veillonella spp.* in the elimination of *S. sanguinis* due to these acidic compounds is considered an inhibiting factor, which is denoted as α_1. This was based on the results in [12], which revealed that the acidic compounds produced by *S. mutans* were broken down into weaker compounds. As a result, the elimination rate of *S. sanguinis* was due to the reduced acidity. In addition, the influence of antibacterials controls the growth of the *S. sanguinis* population, which is denoted as ξ. Furthermore, the difference in antibacterial effectiveness against each bacterium is included in the model. In this case, the antibacterial efficacy against *S. sanguinis* is denoted by a_1.

(2) *S. mutans* population notated by M.

This population is influenced by constant natural growth and death rates, which are denoted as Λ_2 and μ_2, respectively. Nevertheless, according to the limited growth-supporting factors, the carrying capacity for *S. mutans* is involved and denoted as K_m. In addition, the population of *S. mutans* can decrease due to the existence of H_2O_2 released by *S. sanguinis*. In this case, the rate of this phenomenon is denoted as ζ_2. The role of *Veillonella spp.* in the elimination of *S. mutans* due to the compound H_2O_2 is considered an inhibiting factor, which is denoted as α_2. This was declared based on a study by Zhou et al. [51], which revealed that *Veillonella spp.* could break down the H_2O_2 into H_2O and O_2. As a result, the elimination rate of *S. mutans* due to the existence of these compounds was reduced. Finally, the elimination rate due to the use of antibacterials and their effectiveness against *S. mutans* are considered and denoted as ξ and a_2, respectively.

(3) *Veillonella spp.* population notated by V.

This population is influenced by constant natural growth and mortality rates, which are denoted as Λ_3 and μ_3, respectively. Next, the parameter ρ represents the average secretion of compounds by both *S. sanguinis* and *S. mutans* as substrates for *Veillonella spp.* This is under the assumption of point 3, which indicated that the growth of *Veillonella spp.* was highly dependent on the existence of *S. sanguinis* and *S. mutans* bacteria. Furthermore, the growth rate of *Veillonella spp.* follows a Holling type II. In this term, when the combination of *S. mutans* and *S. sanguinis* is small, then the denominator is approximately 1. Consequently, the growth rate is proportional to $\rho(M+S)$, which means that the growth of *Veillonella spp.* increases as *S. mutans* and *S. sanguinis* increase. Alternatively, when the combination of *S. mutans* and *S. sanguinis* is vast, the 1 in the denominator becomes insignificant compared to $\rho(M+S)$. Consequently, the fraction of

$$\rho(M+S)/(1+\rho(M+S))$$

is equal to 1. This causes the growth term to approach a maximum value of $\Lambda_3 V$. In addition, the elimination rate due to the use of antibacterials and their effectiveness against *Veillonella spp.* denoted as ξ and a_3, respectively, are also considered in the model.

Based on the assumptions and descriptions above, the population dynamics of *S. sanguinis*, *S. mutans*, and *Veillonella spp.* can be illustrated as a schematic diagram (Figure 1).

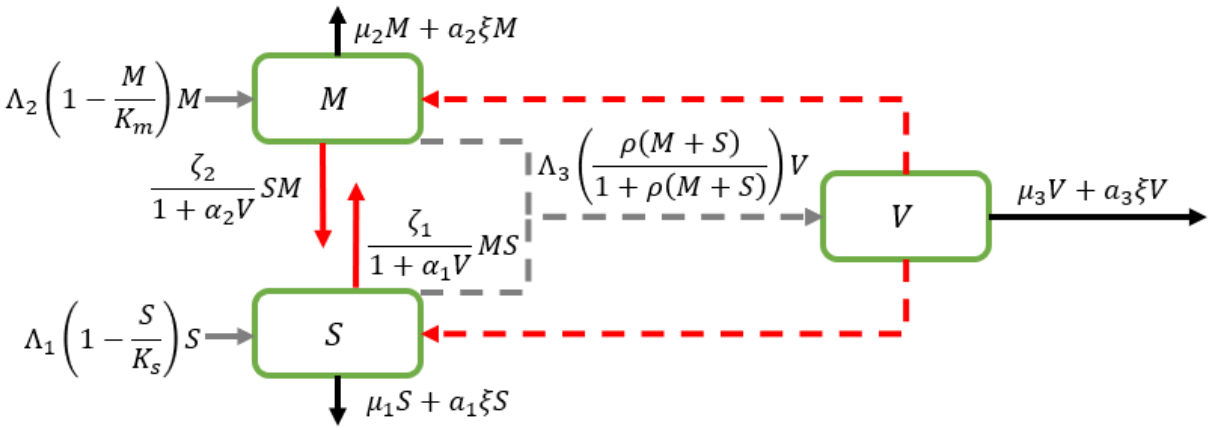

Figure 1. Schematic diagram of bacterial population dynamics.

In Figure 1, the type of line and the associated color represents different conditions. First, the solid grey line represents the growth of both *S. mutans* and *S. sanguinis*. Next, the dashed grey line shows the growth factor of *Veillonella spp.*, which iss influenced by the existence of *S. mutans* and *S. sanguinis*. The solid black line represents the depopulation rate of each bacterium, which is impacted by the natural death rate and the use of antibacterial agents. Next, the dashed red line shows the indirect effect of *Veillonella spp.* existence against the dynamics of *S. mutans* and *S. sanguinis*. Finally, the solid red line represents the depopulation rate of *S. mutans* and *S. Sanguinis* due to their competition between each other while considering the existence of *Veillonella spp.*. Furthermore, in formulating the mathematical model, each factor considered in the study must be defined as a mathematical symbol, which is hereinafter referred to as a parameter. Each parameter and definition used in the model are presented in Table 1.

Table 1. Definition and parameter values of bacterial population dynamics models.

Parameters	Descriptions	Values	Baseline Values	Unit
Λ_1	*S. sanguinis* growth rate	$\frac{3}{10^3}$	$\frac{3}{10^3}$	$\frac{1}{day}$
Λ_2	*S. mutans* growth rate	$\frac{3}{10^3}$	$\frac{3}{10^3}$	$\frac{1}{day}$
Λ_3	*Veillonella spp.* growth rate	$\frac{3}{10^2}$	$\frac{3}{10^2}$	$\frac{1}{day}$
K_s	Carrying capacity of *S. sanguinis*	$\frac{8}{10^2}$	$\frac{8}{10^2}$	Non-dimensional
K_m	Carrying capacity of *S. mutans*			
ζ_1	Elimination rate of *S. sanguinis*	$\frac{3}{10}$	$\frac{3}{10}$	$\frac{1}{\frac{kg}{m^3}\times day}$
ζ_2	Elimination rate of *S. mutans*			
ρ	Secretion rate of compounds by *S. sanguinis* and *S. mutans*	1	1	$\frac{kg}{m^3}$
α_1	The level of influence of the existence of *Veillonella spp*. on the elimination of *S. sanguinis*	$\alpha_1 \in [0,1]$	0.95	$\frac{1}{\frac{kg}{m^3}\times day}$
α_2	The level of influence of the existence of *Veillonella spp*. on the elimination of *S. mutans*	$\alpha_2 \in [0,1]$	1	
ξ	Bacterial elimination rate due to antibacterials	$\frac{3}{10^4}$	$\frac{3}{10^4}$	$\frac{1}{day}$
a_1	Antibacterial effectiveness against *S. sanguinis*	$a_{1,2,3} \in [0,1]$	0.5	Non-dimensional
a_2	Antibacterial effectiveness against *S. mutans*			
a_3	Antibacterial effectiveness against *Veillonella spp.*			
μ_1	Natural mortality rate of *S. sanguinis*	$\frac{3}{10^6}$	$\frac{3}{10^6}$	$\frac{1}{day}$
μ_2	Natural mortality rate of *S. mutans*			
μ_3	Natural mortality rate of *Veillonella spp.*			

The bacterial population dynamics model was formulated as a system of autonomous ordinary differential equations. Based on the descriptions in the previous paragraphs and Figure 1, the autonomous mathematical model can be written as follows:

$$\frac{dS}{dt} = \Lambda_1\left(1-\frac{S}{K_s}\right)S - \frac{\zeta_1}{1+\alpha_1 V}MS - \mu_1 S - a_1\xi S,$$

$$\frac{dM}{dt} = \Lambda_2 \left(1 - \frac{M}{K_m}\right) M - \frac{\zeta_2}{1+\alpha_2 V} SM - \mu_2 M - a_2 \xi M, \tag{1}$$

$$\frac{dV}{dt} = \Lambda_3 \frac{\rho(M+S)}{1+\rho(M+S)} V - \mu_3 V - a_3 \xi V.$$

3. Mathematical analysis

A dynamic analysis of the model includes solution existence, equilibrium solutions, and a stability analysis. However, to simplify the analysis process, system (1) is reformulated into the following:

$$\frac{dS}{dt} = \Lambda_1 \left(1 - \frac{S}{K_s}\right) S - \frac{\zeta}{1+\alpha_1 V} MS - \psi S,$$

$$\frac{dM}{dt} = \Lambda_2 \left(1 - \frac{M}{K_m}\right) M - \frac{\zeta}{1+\alpha_2 V} SM - \psi M, \tag{2}$$

$$\frac{dV}{dt} = \Lambda_3 \frac{\rho(M+S)}{1+\rho(M+S)} V - \psi V,$$

where $\zeta_1 = \zeta_2 = \zeta$, and $\psi = \mu_i + \xi a_i, i = 1,2,3$. Note that the model in system (2) was only used for analysis.

3.1. Properties of solutions

The solution properties were explored to ensure that they satisfied the properties required to be interpreted as a biological problem, namely that they are non-negative and non-negatively invariant for any $t > 0$. This means that a solution to a system (2) with non-negative initial values can remain non-negative for any $t > 0$.

Theorem 1 [53]**.** *The solutions $S(t), M(t)$, and $V(t)$ of the model (2) with non-negative initial values $S(0), M(0)$, and $V(0)$, respectively, can remain non-negative for $t > 0$.*

Proof. Let $t_2 = \sup\{t \in [0,T]: S(0) \geq 0, M(0) \geq 0, V(0) \geq 0\} > 0$. Based on the first equation of system (2), the following formation is considered:

$$\frac{dS}{dt} = \Lambda_1 \left(1 - \frac{S}{K_s}\right) S - \frac{\zeta}{1+\alpha_1 V} MS - \psi S. \tag{3}$$

Using the integrating factor method, the solution for Eq (3) can be written as follows:

$$S(t) \geq \mathcal{C} \exp\left[-\left(\frac{\zeta M}{1+\alpha_1 V(t)} + \psi\right) t\right].$$

$S(0) \geq \mathcal{C}$ is obtained at the initial condition of the model, namely $t = 0$. As a result, the solution dS/dt can be written as follows:

$$S(t_2) \geq S(0) \exp\left[-\left(\frac{\zeta M}{1+\alpha_1 V(t)} + \psi\right) t\right] \geq 0 \; \forall \; t \geq 0.$$

A similar procedure can be used to show that the solutions $M(t_2) \geq 0$ and $V(t_2) \geq 0$ for every $t > 0$. Therefore, it is evident that every model solution for system (2) can remain non-negative when the initial values are non-negative.

The biologic invariant region of system (2) is defined as $\Omega_b = \Omega_s \times \Omega_m \times \Omega_v \subset \mathbb{R}_+ \times \mathbb{R}_+ \times \mathbb{R}_+$, with $\Omega_s = \{S(t) \leq K_s(\Lambda_1 - \psi)/\Lambda_1 \in \mathbb{R}_+\}, \Omega_m = \{M(t) \leq K_m(\Lambda_2 - \psi)/\Lambda_2 \in \mathbb{R}_+\}$, and $\Omega_v = \{V(t) \leq V^* \in \mathbb{R}_+\}$. Therefore, it can be shown that Ω_b is a non-negatively invariant set.

Lemma 2. *The solutions of model (2) are exist, non-negative, unique, and bounded in the region of* Ω_b.

Proof. The invariant region for system (2) can be determined by utilizing the box invariant method, which was also used in [54,55]. The compact form of system (2) can be expressed as follows:

$$\frac{d\boldsymbol{X}}{dt} = \boldsymbol{A}(\boldsymbol{X})\boldsymbol{X} + \boldsymbol{F},$$

where $\boldsymbol{X} = [S, M, V]^T$, and $\boldsymbol{F}$ are column vectors that can be written as follows:

$$\boldsymbol{F} = \left[\Lambda_1\left(1 - \frac{S}{K_s}\right)S, \Lambda_2\left(1 - \frac{M}{K_m}\right)M, \Lambda_3\frac{\rho(S+M)}{1+\rho(S+M)}\right]$$

and

$$\boldsymbol{A}(\boldsymbol{X}) = \begin{bmatrix} -\psi - \dfrac{\zeta}{1+\alpha_1 V}M & 0 & 0 \\ 0 & -\psi - \dfrac{\zeta}{1+\alpha_2 V}S & 0 \\ 0 & 0 & -\psi \end{bmatrix}.$$

These show that $\boldsymbol{A}(\boldsymbol{X})$ is a Metzler matrix for every $\boldsymbol{X} \in \mathbb{R}^3$, since Theorem 1 guarantees that S and M are non-negative for every $t > 0$ with non-negative initial values. Furthermore, by the column vector $F \geq 0$, the model solutions to system (2) are non-negative in $\mathbb{R}^3$. Any path of solution to system (2) in $\mathbb{R}^3_+$ can remain in $\mathbb{R}^3_+$, therefore, Ω_b is non-negatively invariant for $t > 0$.

Next, to ensure the existence and uniqueness of the solution, Picard's theorem is utilized. Nevertheless, we tried to ensure that $d\mathbf{X}/dt$ is locally Lipschitz. A well-known way to prove this is to show that $d\mathbf{X}/dt$ is continuously differentiable (a C^1 function). In this term, we can see that the functions are nonlinear, and the partial derivative of each element of $d\mathbf{X}/dt$ is continuously differentiable and equal to zero. Nevertheless, in this model, the denominators are $(1 + \alpha_1 V), (1 + \alpha_2 V)$, and $\big(1 + \rho(M + S)\big)$, Assuming the population of $S, M,$ and V with α_1, α_2 and ρ are non-negative. Hence, the denominators are always greater than or equal to 1 and are never zero, since all partial derivatives of $d\mathbf{X}/dt$ are continuously differentiable and locally Lipschitz continuous.

All functions expressed in the right-hand side of model (2) are C^1 on $\mathbb{R}^3_+$. Regarding Picard's theorem, model (2) has a unique solution. Let the model be rewritten as $y' = g\,(y, t)$, where $y = (S, M, V)$ and g is the right-hand side. According to the results of Picard's theorem, the function of $g(y, t)$ fulfills Theorem 1. Since there exists a unique solution for model (2), then $y(t) \in [0, \infty]^3$ holds for all $t > 0$ whenever $y(0) > 0$. The rate of change of each bacterium is equal to the expressed equations in (2). Solving each equation in model (2) results in the following solutions:

$$S(t) \leq \frac{K_s\left(1-\frac{\psi}{\Lambda_1}\right)}{1+\left(\frac{K_s\left(1-\frac{\psi}{\Lambda_1}\right)-S(0)}{S(0)}\right)e^{-\left(\Lambda_1-\psi\right)t}},$$

$$M(t) \leq \frac{K_m\left(1-\frac{\psi}{\Lambda_2}\right)}{1+\left(\frac{K_m\left(1-\frac{\psi}{\Lambda_2}\right)-M(0)}{M(0)}\right)e^{-\left(\Lambda_2-\psi\right)t}},$$

and $V(t) \leq V^*$. Therefore, for any non-negative initial condition, the following result hold:

$$0 \leq S(t) \leq K_s\left(1-\frac{\psi}{\Lambda_1}\right),$$

$$0 \leq M(t) \leq K_m\left(1-\frac{\psi}{\Lambda_2}\right),$$

and $0 \leq V(t) \leq V^*$. This implies that the solution of model (2) exists, is unique, and is bounded in Ω_b. Finally, we conclude that the model is well-posed.

Based on Theorem 1 and Lemma 2, it could be concluded that the solution obtained from system (2) represents a biological problem.

3.2. Equilibrium solution

The equilibrium solution is obtained when the rate of change of each bacterial population in system (2) is equivalent to zero, namely a condition where the population of each bacteria for $t > 0$ is the same. There were 5 equilibrium solutions obtained from system (2), which are described below.

(1) The trivial solution represents the condition where all observed bacteria are not growth and tend to extinction. This solution can be written as follows:

$$\Upsilon_0 = \{S^* = 0, M^* = 0, V^* = 0\}.$$

(2) Non-trivial solution 1 represents the condition where only *S. sanguinis* bacteria can survive in the biofilm, while *S. mutans* and *Veillonella spp.* head toward extinction. This solution can be written as follows:

$$\Upsilon_1 = \left\{S^* = K_s\frac{(\Lambda_1-\psi)}{\Lambda_1}, M^* = 0, V^* = 0\right\}.$$

(3) Non-trivial solution 2 represents the condition where only *S. mutans* bacteria can survive in the biofilm, while *S. sanguinis* and *Veillonella spp.* head toward extinction. This solution can be written as follows:

$$\Upsilon_2 = \left\{S^* = 0, M^* = K_m \frac{(\Lambda_2 - \psi)}{\Lambda_2}, V^* = 0\right\}.$$

(4) Non-trivial solution 3 represents the condition where only *S. sanguinis* and *S. mutans* bacteria can survive in the biofilm, while *Veillonella spp.* head toward extinction. This solution can be written as follows:

$$\Upsilon_3 = \left\{S^* = K_s \frac{K_m\zeta(\Lambda_2 - \psi) + (\psi - \Lambda_1)\Lambda_2}{K_m K_s\zeta^2 - \Lambda_1\Lambda_2}, M^* = K_m \frac{K_s\zeta(\Lambda_1 - \psi) + (\psi - \Lambda_2)\Lambda_1}{K_m K_s\zeta^2 - \Lambda_1\Lambda_2}, V^* = 0\right\}.$$

(5) The interior solution represents the conditions under which each bacterium can survive in the biofilm, and this can be written as follows:

$$\Upsilon_4 = \{S^*, M^*, V^*\}$$

where

$$S^* = \frac{K_s}{(K_m K_s\zeta^2 - (1 + \alpha_1 V^*)(1 + \alpha_2 V^*)\Lambda_1\Lambda_2)\Lambda_1}\Big(\big((1 + \alpha_2 V^*)(\alpha_1\eta V^* + K_m\zeta + \eta)\Lambda_2 - (\alpha_2\zeta\eta V^* + \zeta\eta)K_m\big)\Lambda_1 - (1 + \alpha_1 V^*)(1 + \alpha_2 V^*)\Lambda_2\Lambda_1^2\Big),$$

$$M^* = K_m \frac{(1 + \alpha_1 V^*)\big((\alpha_2(\eta - \Lambda_2)V^* + \eta - \Lambda_2)\Lambda_1 - K_s\zeta(\Lambda_1 - \eta)\big)}{K_m K_s\zeta^2 - (1 + \alpha_1 V^*)(1 + \alpha_2 V^*)\Lambda_1\Lambda_2},$$

and V^* is a positive root of the quadratic equation $P(V^*)$, which can be written as follows:

$$P(V^*) = \frac{x_2(V^*)^2 + x_1 V^* + x_0}{y_2(V^*)^2 + y_1 V^* + y_0},$$

with

$$x_2 = \alpha_1\alpha_2\Big((\Lambda_3 - \eta)\big((K_m\eta - (K_m + K_s)\Lambda_2)\Lambda_1 + K_s\eta\Lambda_2\big)\rho + K_v\eta\Lambda_1\Lambda_2\Big),$$

$$x_1 = \Lambda_1\Lambda_2 K_v\eta(\alpha_1 + \alpha_2) - (\Lambda_3 - \eta)\Big((-K_m(\alpha_1 + \alpha_2)\Lambda_1 + (\alpha_1 + \alpha_2)(K_m\zeta - \Lambda_2)K_s)\eta + \big((K_m + K_s)(\alpha_1 + \alpha_2)\Lambda_2 - K_m K_s\zeta\alpha_1\big)\Lambda_1 - K_m K_s\zeta\alpha_2\Lambda_2\Big)\rho,$$

$$x_0 = (\Lambda_1\Lambda_2 - K_m K_s\zeta^2)K_v\eta - \Big(\big((2\zeta K_s - \Lambda_1)K_m - K_s\Lambda_2\big)\eta + (\Lambda_1\Lambda_2 - (\Lambda_1 + \Lambda_2)\zeta K_s)K_m + K_s\Lambda_1\Lambda_2\Big)(\Lambda_3 - \eta)\rho,$$

$$y_2 = \alpha_1\alpha_2\big((K_m\eta\rho - (K_v + (K_m + K_s)\rho)\Lambda_2)\Lambda)1 + K_s\eta\rho\Lambda_2\big),$$

$$y_1 = \Big(\big((K_m\zeta\alpha_2 + (\alpha_1 + \alpha_2)\eta)\Lambda_2 - (\alpha_1 + \alpha_2)K_m\eta\zeta\big)K_s - \big((K_m + K_s)(\alpha_1 + \alpha_2)\Lambda_2 - (K_s\zeta\alpha_1 + (\alpha_1 + \alpha_2)\eta)K_m\big)\Lambda_1\Big)\rho - (\alpha_1 + \alpha_2)\Lambda_1\Lambda_2 K_v,$$

$$y_0 = (K_m K_s\zeta^2 - \Lambda_1\Lambda_2)K_v - \Big(\big((2\eta\zeta - (\Lambda_1 + \Lambda_2)\zeta)K_s + \Lambda_1(\Lambda_2 - \eta)\big)K_m + (\Lambda_1 - \eta)\Lambda_2 K_s\Big)\rho.$$

Using the Descartes law of signs, the solution of $P(V^*)$ can be elaborated as in Table 2.

Table 2. Possible many positive roots $P(V^*)$.

Condition	x_2	x_1	x_0	Many positive roots
1	+	+	+	0
2	+	+	−	1
3	+	−	+	0 or 2
4	+	−	−	1
5	−	+	+	1
6	−	+	−	0 or 2
7	−	−	+	1
8	−	−	−	0

These lead to the conclusion that $P(V^*)$ has at least a positive root if $x_2 > 0$ and $x_0 < 0$ or $x_2 < 0$ and $x_0 > 0$. Consequently, system (2) has a solution Υ_4 and at least has a non-negative solution for $t > 0$.

3.3. Stability analysis

The stability analysis of model solutions is considered by revealing the eigenvalues from the Jacobian matrix, denoted as $\boldsymbol{J}$, of system (2), which is substituted by $\Upsilon_0, \Upsilon_1, \Upsilon_2,$ and Υ_3. The analysis for each solution is described below.

(1) Stability of the trivial solution (Υ_0)

The eigenvalues of $\boldsymbol{J}(\Upsilon_0)$ can be determined by finding the solution λ for $\det(\boldsymbol{J}(\Upsilon_0) - \lambda \boldsymbol{I}) = 0$, which leads to the following:

$$\lambda_1 = \Lambda_1 - \psi, \qquad \lambda_2 = \Lambda_2 - \psi, \qquad \lambda_3 = -\psi.$$

As a result, the stability of the solution Υ_0 can reach two conditions with the following criteria:

- Υ_0 is unstable when $\Lambda_1 > \psi$ and $\Lambda_2 > \psi$, then $\lambda_1, \lambda_2 > 0$, while λ_3 is always negative, or
- Υ_0 is stable when $\Lambda_1 < \psi$ and $\Lambda_2 < \psi$, then $\lambda_1, \lambda_2, \lambda_3 < 0$.

(2) Stability of non-trivial solution 1 (Υ_1)

The eigenvalues of $\boldsymbol{J}(\Upsilon_1)$ can be determined by finding the solution λ for $\det(\boldsymbol{J}(\Upsilon_1) - \lambda I) = 0$, which leads to the following:

$$\lambda_1 = -\Lambda_1 + \psi, \qquad \lambda_2 = \frac{K_s\zeta(-\Lambda_1 + \psi) + (-\psi + \Lambda_2)\Lambda_1}{\Lambda_1},$$

$$\lambda_3 = \frac{K_s\rho(-\Lambda_1 + \psi)(-\psi + \Lambda_3) + \eta\Lambda_1}{K_s\rho(-\Lambda_1 + \psi) - \Lambda_1}.$$

Consequently, Υ_1 can reach the stability condition when $\Lambda_1 > \psi > \Lambda_2, \Lambda_3$, which makes $\lambda_1, \lambda_2, \lambda_3 < 0$ and unstable for the others.

(3) Stability of non-trivial solution 2 (Υ_2)

The eigenvalues of $\boldsymbol{J}(\Upsilon_2)$ can be determined by finding the solution λ for

$$\det(\boldsymbol{J}(\Upsilon_2) - \lambda I) = 0,$$

which leads to the following:

$$\lambda_1 = \frac{K_m\zeta(-\Lambda_2 + \psi) + (-\psi + \Lambda_1)\Lambda_2}{\Lambda_2}, \qquad \lambda_2 = -\Lambda_2 + \psi,$$

$$\lambda_3 = \frac{K_m\rho(-\Lambda_2 + \psi)(-\psi + \Lambda_3) + \eta\Lambda_2}{K_m\rho(-\Lambda_2 + \psi) - \Lambda_2}.$$

Consequently, Υ_2 will reach the stability condition if $\Lambda_2 > \psi > \Lambda_1, \Lambda_3$, which makes $\lambda_1, \lambda_2, \lambda_3 < 0$ and unstable for the others.

(4) Stability of non-trivial solution 3 (Υ_3)

The eigenvalues of $\boldsymbol{J}(\Upsilon_3)$ can be determined by finding the solution λ for $\det(\boldsymbol{J}(\Upsilon_3) - \lambda I) = 0$. The determination of the eigenvalues of the matrix $\boldsymbol{J}(\Upsilon_3)$ is not similar to the previous matrix. This is more complicated and requires a separate step. In this case, the first 2 eigenvalues are expressed as follows:

$$f(\lambda) = a\lambda^2 + b\lambda + c$$

with

$$a = (K_sK_m\zeta^2 - \Lambda_1\Lambda_2),$$

$$b = \Big(\big((K_s + K_m)\zeta + 2\psi\big) - (\Lambda_1 + \Lambda_2)\Big)\Lambda_1\Lambda_2 - (K_m\Lambda_1 + K_s\Lambda_2)\psi\zeta,$$

$$c = \big((\Lambda_1 - \psi)\Lambda_2 - (\Lambda_2 - \psi)K_m\zeta\big)\big((\Lambda_2 - \psi)\Lambda_1 - (\Lambda_1 - \psi)K_s\zeta\big).$$

Considering Descartes' rule, two negative eigenvalues as solutions of $f(\lambda) = 0$ can only be obtained when $a, b, c > 0$. Furthermore, the third eigenvalue for $\det(\boldsymbol{J}(\Upsilon_3) - \lambda I) = 0$ can be written as follows

$$\lambda_3 = \frac{(\Lambda_3 - \psi)d - \eta a}{d - a}$$

with

$$d = \rho\left(K_s\Lambda_2(\psi - \Lambda_1) - \left(2K_s\zeta\left(\psi - \left(\frac{\Lambda_1 + \Lambda_2}{2}\right)\right) + (\Lambda_2 - \psi)\Lambda_1\right)K_m\right).$$

Next, the final exploration required to assume the stability of the solution Υ_3 is to show that $\lambda_3 < 0$. Consequently, $K_sK_m\zeta^2 - \Lambda_1\Lambda_2$ must be greater than zero. Since this solution indicates the extinction of *Veillonella spp.*, Λ_3 must be less than ψ. Consequently, $\Lambda_3 - \psi$ is negative, therefore, the solution Υ_3 is stable.

(5) Stability of interior solution (Υ_4)

Next, we perform a global stability analysis around the interior equilibrium solution Υ_4. This can

be explored using the Lyapunov function and LaSalle's invariance principle. First, the Lyapunov formulation for system (2) that was used can be written as follows:

$$L(S,M,V) = \left(S - S^* - S^* \ln\frac{S}{S^*}\right) + \left(M - M^* - M^* \ln\frac{M}{M^*}\right) + \left(V - V^* - V^* \ln\frac{V}{V^*}\right)$$

where r_1 and r_2 are arbitrary positive constants. The derivative of L with respect to t results in the following:

$$\frac{dL}{dt} = \left(1 - \frac{S^*}{S}\right)\frac{dS}{dt} + \left(1 - \frac{M^*}{M}\right)\frac{dM}{dt} + \left(1 - \frac{V^*}{V}\right)\frac{dV}{dt}. \tag{4}$$

By substituting system (2) into Eq (4) and looking at $S^*, M^*,$ and V^* as a set of equilibrium solutions, the following equation is produced:

$$\frac{dL}{dt} = (S - S^*)\left[\Lambda\left(1 - \frac{S}{K_S}\right) - \frac{\zeta}{1 + \alpha_1 V}M - \psi\right] + (M - M^*)\left[\Lambda_2\left(1 - \frac{M}{K_M}\right) - \frac{\zeta}{1 + \alpha_2 V}S - \psi\right]$$

$$+(V - V^*)\left[\Lambda_3 \frac{\rho(M+S)}{1+\rho(M+S)} - \psi\right]. \tag{5}$$

By performing several algebra manipulations (see Appendix A), Equation (5) can be rewritten as follows:

$$\frac{dL}{dt} = -\frac{\Lambda_1}{K_s}(S - S^*)^2 - \frac{\Lambda_2}{K_m}(M - M^*)^2 - \left[\frac{\zeta}{1 + \alpha_1 V^*} + \frac{\zeta}{1 + \alpha_2 V^*}\right](S - S^*)(M - M^*)$$

$$+\Lambda_3\left[\frac{\rho(M+S)}{1+\rho(M+S)} - \frac{\rho(S^*+M^*)}{1+\rho(S^*+M^*)}\right](V - V^*). \tag{6}$$

The function dL/dt in Eq (6) can be negative when $V(t) = V^*$. Consequently, the function L is proven to be a Lyapunov function for system (2). Thus, using LaSalle's invariance principle, it can be concluded that the solution Υ_4 is globally asymptotically stable on Ω_b. Based on this result, Theorem 3 holds.

Theorem 3. *An interior solution of* Υ_4 *is globally asymptotically stable when* $V(t) = V^*$.

4. Sensitivity analysis

In this section, a sensitivity analysis is performed to explore the influence of each considered factor on the caries threshold and reveals the role of *Veillonella spp.* in caries formation from a mathematical perspective. The Latin Hypercube Sampling (LHS) [56] is utilized to conduct the sensitivity analysis to generate the sample. Next, we use the Partial Rank Correlation Coefficient (PRCC) [56] to identify the correlation and its rank. The analysis begins by assuming that the value of $\zeta = \zeta_1 = \zeta_2$. This analysis of bacterial population dynamics in oral biofilms is conducted at the threshold of dental caries risk. In the case studied, referring to the definition expressed in [52], the threshold of dental caries risk is denoted as ς and can be formulated as follows:

$$\varsigma = \frac{\left(K_s\zeta\left(\Lambda_1 - (\mu_1 - \xi a_1)\right) - (1 + \alpha_2 V^*)\left(\Lambda_2 - (\mu_2 - \xi a_2)\right)\Lambda_1\right)}{\left(K_m\zeta\left(\Lambda_2 - (\mu_2 - \xi a_2)\right) - (1 + \alpha_1 V^*)\left(\Lambda_1 - (\mu_1 - \xi a_1)\right)\Lambda_2\right)} \times \frac{K_m}{K_s}\frac{(1 + \alpha_1 V^*)}{(1 + \alpha_2 V^*)}.$$

The results of the sensitivity analysis on the dental caries risk threshold are presented in Figure 2.

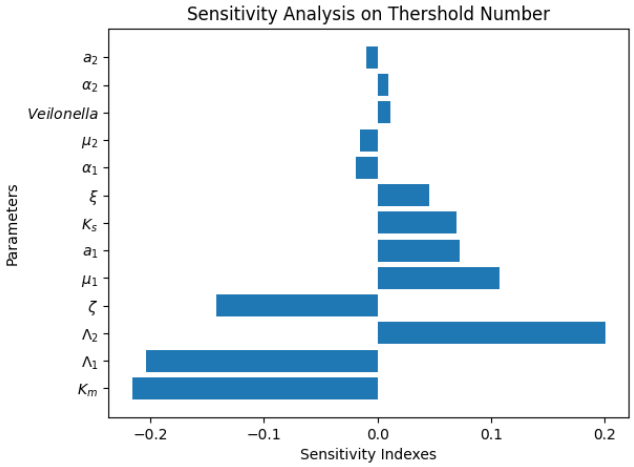

Figure 2. The sensitivity value of each parameter to dental caries risk threshold ς.

Figure 2 shows that the carrying capacity for *S. mutans* (K_m), the recruitment rate of *S. sanguinis* (Λ_1), the effect of *Veillonella spp.* on the elimination of *S. sanguinis* (α_1), and the effectiveness of antibacterial against *S. mutans* (a_2) are factors that are negatively correlated with the threshold, that is, each decrease in the value of these parameters caused the threshold to increase. Meanwhile, the existence of *Veillonella spp.* is positively correlated with the threshold of dental caries risk. In this case, *Veillonella spp.* tends to support the growth of *S. mutans* in oral biofilms and the risk of dental caries formation increases. These results support the results in [52] and [13], which revealed that *Veillonella spp.* was positively correlated with the existence of dental caries.

5. Optimal control model

This section describes the optimal control theory on the population dynamics model of bacteria in oral biofilms. The optimal control problem is applied to measure the need for antibacterial use to suppress the population of each bacterium and control the ratio $\varsigma < 1$. The control variables denoted by $a_b(t)$ were viewed as multipliers on ξa_i where $i = 1,2,3$. The optimal control model was constructed to minimize each bacterium's population and antibacterial use. Therefore, the objective function for the optimal control problem of the bacterial population dynamics model can be formulated as follows:

$$Jc(a_b) = \int_0^{t_f} A_2\left(S(t) + M(t) + V(t)\right) + C_2\left(a_b(t)\right)^2 dt. \tag{7}$$

Parameters A_2 and C_2 represent the weight value for each bacterial population and the cost measure of antibacterial use, respectively. The optimal control model for the dynamic problem of bacterial populations in oral biofilms can be formulated by considering the objective function (7) and

the dynamic model (1), which is written as follows:

$$Jc(a_b^*) = \int_0^{t_f} A_2\big(S(t) + M(t) + V(t)\big) + C_2\big(a_b(t)\big)^2\, dt,$$

$$s.t. \frac{dS}{dt} = \Lambda_1\left(1 - \frac{S}{K_s}\right)S - \frac{\zeta_1}{1+\alpha_1 V}MS - \mu_1 S - a_b(t)a_1\xi S, \tag{8}$$

$$\frac{dM}{dt} = \Lambda_2\left(1 - \frac{M}{K_m}\right)M - \frac{\zeta_2}{1+\alpha_2 V}SM - \mu_2 M - a_b(t)a_2\xi M,$$

$$\frac{dV}{dt} = \Lambda_3\frac{\rho(M+S)}{1+\rho(M+S)}V - \mu_3 V - a_b(t)a_3\xi V.$$

It is known that $S(0) \geq 0, M(0) \geq 0, V(0) \geq 0, 0 \leq t \leq t_f$, and $0 \leq a_b(t) \leq 1$.

Based on Eq (7), the optimal value of $a_b(t)$ is determined by numerical calculation, which is formulated as follows: $Jc(a_b^*) = \min_U\{J(a_b)\}$, where $U = \{a_b : [0, t_f] \to [0,1]\}$. The Hamiltonian equation for the optimal control problem (8) can be formulated as follows:

$$H = A_2\big(S(t) + M(t) + V(t)\big) + \lambda_1(t)\frac{dS(t)}{dt} + \lambda_2(t)\frac{dM(t)}{dt} + \lambda_3(t)\frac{dV(t)}{dt} \tag{9}$$

where $\lambda_{1,2,3} \geq 0$ respectively defines the adjoint variables for S, M, and V. Next, the adjoint functions are obtained from the partial derivative of H against S, M, and V, which can be written as follows:

$$\dot{\lambda}_1(t) = -A_2 - \left(-a_1\xi a_b(t) - \mu_1 - \frac{\zeta_1 M(t)}{1+\alpha_1 V(t)} + \Lambda_1\left(1 - \frac{S(t)}{K_s}\right) - \frac{\Lambda_1 S(t)}{K_s}\right)\lambda_1(t) + \frac{\xi M(t)}{1+\alpha_2 V(t)}\lambda_2(t)$$
$$-\left(-\frac{\rho^2\Lambda_3\big(S(t)+M(t)+V(t)\big)}{\big(1+\rho\big(S(t)+M(t)\big)\big)^2} + \frac{\rho\Lambda_3 V(t)}{1+\rho\big(S(t)+M(t)\big)}\right)\lambda_3(t),$$

$$\dot{\lambda}_2(t) = -A_2 + \frac{\xi S(t)}{1+\alpha_1 V(t)}\lambda_1(t) - \left(-a_2\xi a_b(t) - \mu_2 - \frac{\zeta_2 S(t)}{1+\alpha_2 V(t)} + \Lambda_2\left(1 - \frac{M(t)}{K_s}\right) - \frac{\Lambda_2 M(t)}{K_m}\right)\lambda_2$$
$$-\left(\frac{\rho^2\Lambda_3\big(M(t)+S(t)\big)V(t)}{\big(1+\rho\big(S(t)+M(t)\big)\big)^2} + \frac{\rho\Lambda_3 V(t)}{1+\rho\big(S(t)+M(t)\big)}\right)\lambda_3(t),$$

$$\dot{\lambda}_3(t) = -A_2 - \frac{\alpha_1\zeta_1 S(t)M(t)}{\big(1+\alpha_1 V(t)\big)^2}\lambda_1(t) - \frac{\alpha_2\zeta_2 S(t)M(t)}{\big(1+\alpha_2 V(t)\big)^2}\lambda_2(t)$$
$$-\left(-a_3\xi a_b(t) - \mu_3 + \frac{\rho\Lambda_3\big(S(t)+M(t)\big)}{1+\rho\big(S(t)+M(t)\big)}\right)\lambda_3(t),$$

where the final condition for each adjoint variable must be satisfy $\dot{\lambda}_i(t_f) = 0$ for $i = 1,2,3$. The necessary and sufficient conditions for the optimal control problem are obtained, which give the

optimal solution and can be expressed as follows:

$$a_b^*(t) = \min\left\{\max\left\{0, \frac{\xi\left(a_1 S(t)\lambda_1(t) + a_2 M(t)\lambda_2(t) + a_3 V(t)\lambda_3(t)\right)}{2C_2}\right\}, 1\right\}.$$

6. Numerical simulation and its discussion

Numerical simulations are conducted to confirm the analysis results and provide projections of the population dynamics represented by the model in systems (1) and (8). The values presented in Table 1 are the parameter values that were used. However, several selected parameters were varied in value for exploration purposes and can present various projections of population dynamics for each bacterium. The parameters whose values were varied were those that were related to each other, including the effect of the existence of *Veillonella spp.* on the elimination of *S. sanguinis* (α_1) and *S. mutans* (α_2), as well as the antibacterial activity against each bacterium (a_1, a_2, a_3).

The variation of α_1 and α_2 values aimed to show the significance of the difference in ς values due to the significant difference between α_1 and α_2. The results from this simulation can be used to determine how important the selection of antibacterials is to optimize control. The variations of the values are presented in Table 3.

Table 3. Variation of α_1 and α_2 values.

Value / Condition	Parameters	
	α_1	α_2
I	0.95	1
II	0.75	1
III	0.5	1

The variations of a_1, a_2, and a_3 represents the different types of antibacterial influence coefficients. In this case, each product that offered control of bacterial growth in oral biofilms had a distinct impact on each bacterium. For example, 2 bacterial controlled products, X and Y, were given. Product X had an advantage in eliminating *S. mutans* but was weak in eliminating *Veillonella spp.*. Meanwhile, product Y had the advantage of eliminating *Veillonella spp.* but was weak in eliminating *S. mutans*. As a result, these conditions certainly needed to be interpreted as different parameter values. The variations of a_1, a_2, and a_3 values are presented in Table 4.

Table 4. Variation of $a_1, a_2,$ and a_3 values.

Value / Scenario	Parameters		
	a_1	a_2	a_3
I	1	0.75	0.5
II	0.5	1	0.75
III	0.75	0.5	1
IV	1	0.5	0.75
V	0.75	1	0.5
VI	0.5	0.75	1

Numerical simulations are performed using predetermined parameter values. In addition to parameters $\alpha_1, \alpha_2, a_1, a_2,$ and a_3, the values of each parameter used in this simulation are based on the basic values in Table 1. Finally, the initial values of each population are selected as $S(0) = M(0) = V(0) = 0.05\ \text{kg/m}^3$ for every simulation.

All simulations were conducted using Python 3.9. The ordinary differential equations system (ODEs) is solved using the solve_ivp function from the SciPy library. It employs a high-quality Runge-Kutta method (specifically, the Dormand-Prince method of order 5(4)) and equips an adaptive step-size control to ensure the accuracy of the resulting solutions. The absolute error tolerance of 10^{-5} was used for all simulations.

Figure 3 shows that the difference between the values of α_1 and α_2 played a crucial role in the dynamics of the *S. sanguinis* and *S. mutans* populations.

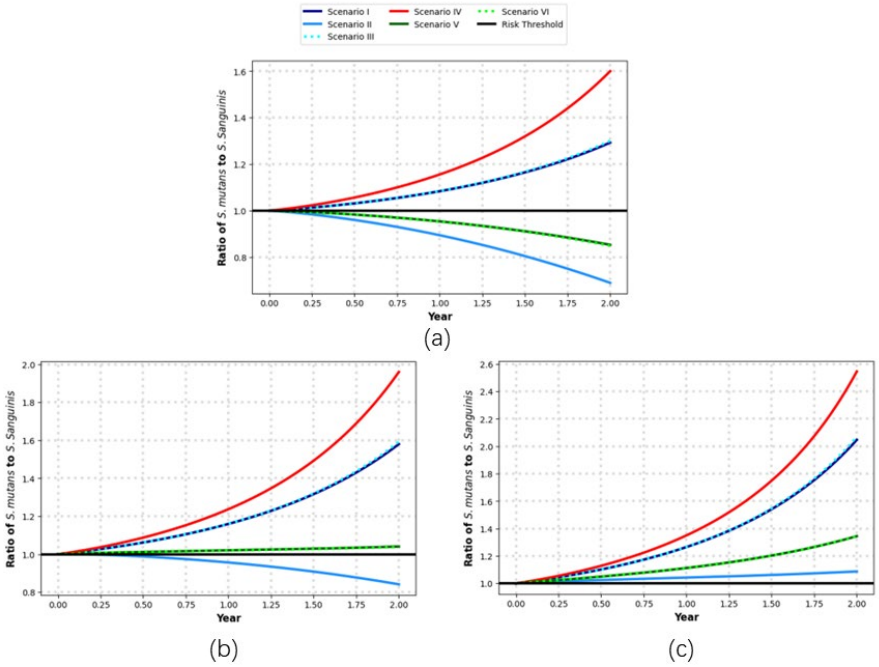

Figure 3. The dynamics of the population ratio of *S. mutans* to *S. sanguinis* under (a) condition I, (b) condition II, and (c) condition III, and the variations in the values of α_1, α_2, and a_3 are presented in Table 4.

In this case, the risk thresholds for the resulting dental caries were different. The simulation results illustrate that when the difference between α_1 and α_2 is insignificant, as presented in Figure 3(a), the threshold projection is divided into 2. First, in conditions $a_1 > a_2$, the caries risk is seen to move away from the caries risk threshold. Meanwhile, in the condition $a_1 < a_2$ moves away from the caries risk threshold. This can be interpreted from the values used in Table 4. The condition $a_1 > a_2$, namely the effectiveness of antibacterial scenarios I, III, and IV, reflects that the antibacterial is more dominant in eliminating the *S. sanguinis* population than the *S. mutans* population. In this condition, the population level of *S. sanguinis* is lower than the population of *S. mutans* in the oral biofilm. As a result, the risk of dental caries increases. The condition $a_1 < a_2$ reflectes the influence of more dominant antibacterials in eliminating *S. mutans* than *S. sanguinis*, and the risk of caries is lower. However, suppose the difference between the influence of *Veillonella spp.* on the elimination rate of *S. mutans*

and *S. sanguinis* is significant, then the risk of dental caries can be increasingly difficult to control. This is shown by the transition of caries risk with the influence of antibacterial scenarios V and VI from Figure 3(a) to Figure 3(b). In the scenario presented, the most severe condition occurs when the difference between α_1 and α_2 is 0.5. This condition results in all antibacterials being unable to control the risk of caries to remain below the risk threshold.

A numerical simulation for the optimal control problem was conducted to compare the projection of dental caries risk without and with the use of antibacterial agents. The scenario without using bacteria is represented by the control variable set to zero in the observation period. Meanwhile, the scenario using antibacterial is represented by the optimal value of the control variable that satisfies the solution of $a_b^*(t)$. An optimal control simulation was conducted for condition II in Table 3 with variations in the values of $a_1, a_2,$ and a_3, which refer to antibacterial scenarios II, V, and VI. Antibacterial scenarios I, III, and IV were no longer considered because each of these antibacteria were dominant in eliminating *S. sanguinis* than *S. mutans*, and the caries risk was higher. Furthermore, an arbitrary boosting factor is considered in the effectiveness of the antibacterial effect. In this case, the boosting factor is reflected as a multiplier of the parameter ξ, which defines the rate of bacterial elimination due to the antibacterial. In addition, to ensure the stability of the upcoming result, we try to conduct multiple runs of each case, thereby considering the variation of the Λ_2 parameter, which is chosen based on the results of the sensitivity analysis, which show that the parameter is most positively correlated with ς. The results of the optimal control simulation are presented in Figure 4.

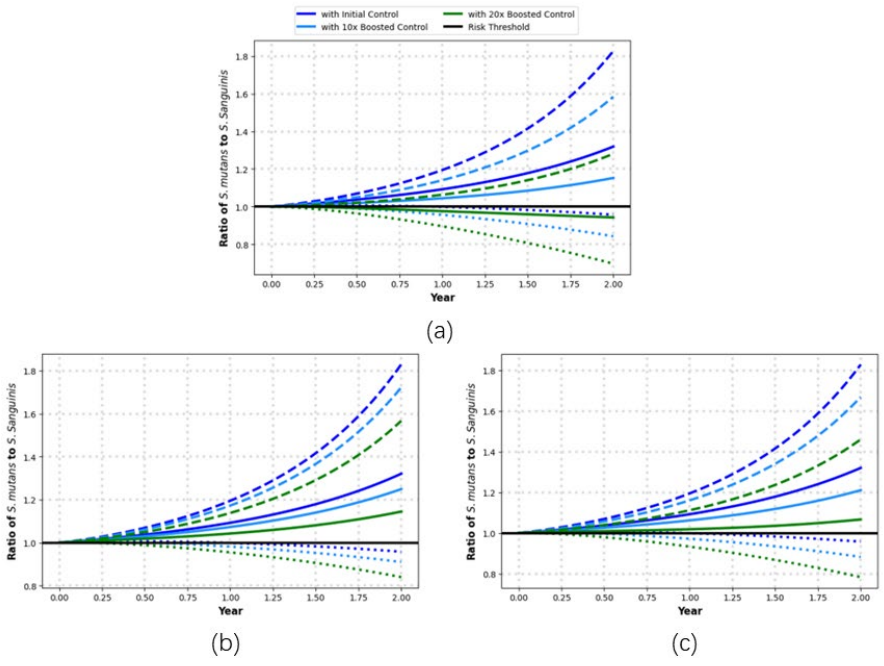

Figure 4. Dynamics of the population ratio of *S. mutans* to *S. sanguinis* under condition II with the influence of antibacterial (a) scenario II, (b) scenario V, and (c) scenario VI. Within each result, the solid line represents the baseline, while dotted and dashed lines correspond to a 5% decrease and increase in Λ_2, respectively.

Based on Figure 4, the control treatment results in a difference in the risk of dental caries, as reflected by the ratio of *S. mutans* to *S. sanguinis*. Each antibacterial has a similar effect on the dynamics of caries risk. Note that the significant difference between a_1 and a_2 provide different control results. This can be concluded by observing the conditions between Figure 4(a–c). In this case, scenario II antibacterial has twice the ability to eliminate *S. mutans* compared to *S. sanguinis*. As a result, the risk of caries can be controlled more effectively. Similar results were not obtained when scenario V and VI antibacterials were used to reduce caries risk. An interesting finding to note is the difference in risk due to the use of scenarios V and VI. Table 4 shows that the difference between a_1 and a_2 indicates the same value, which is 0.25. However, the obtained projection of the dynamics of caries risk is different. This needs to be explored further because scenario VI has twice the ability to eliminate *Veillonella spp*. more effectively than scenario V antibacterials.

Figure 5 indicates the dynamics of the *Veillonella spp.* population in oral biofilms. Figure 5(c) shows a reflection of the dynamics of *Veillonella spp.* due to the use of antibacterial, in which scenario VI was the best way to suppress the *Veillonella spp.* population. These results confirm the difference between Figure 4(b) and 4(c), namely, the risk of dental caries is lower when antibacterial scenario VI is used as an intervention effort compared to scenario V. Furthermore, Figure 5 shows that the use of antibacterial scenario VI can eliminate *Veillonella spp.* better than scenario V. The effect of antibacterial scenario II is better than scenario V, but not better than scenario VI. The results presented in Figure 5 strengthen the sensitivity analysis results, which show that the existence of *Veillonella spp.* is positively correlated with an increased risk of dental caries.

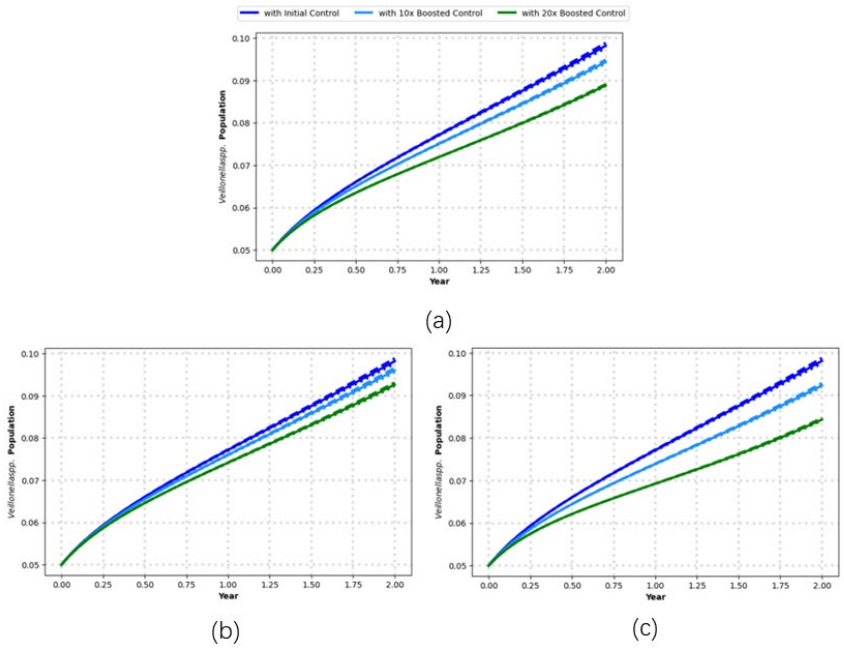

Figure 5. Dynamics of the population ratio of *Veillonella spp.* under condition II with the influence of antibacterial (a) scenario II, (b) scenario V, and (c) scenario VI. Within each result, the solid line represents the baseline, while dotted and dashed lines correspond to a 5% decrease and increase in Λ_2, respectively.

Figure 6 shows that the use of each antibacterial scenario is different, which can be interpreted as the number of antibacterials and the duration of their use in controlling the risk of dental caries. The use of antibacterials in scenarios II and VI are similar, namely antibacterials with a twenty-fold boosting factor are the most widely used. Meanwhile, scenario V results in antibacterials with a ten-fold boosting factor having been the most commonly used in reducing the risk of caries. Based on the results in Figures 4–6, it could be concluded that antibacterial control helps control the growth of *S. sanguinis*, *S. mutans*, and *Veillonella spp.* in oral biofilms and reduces the risk of dental caries.

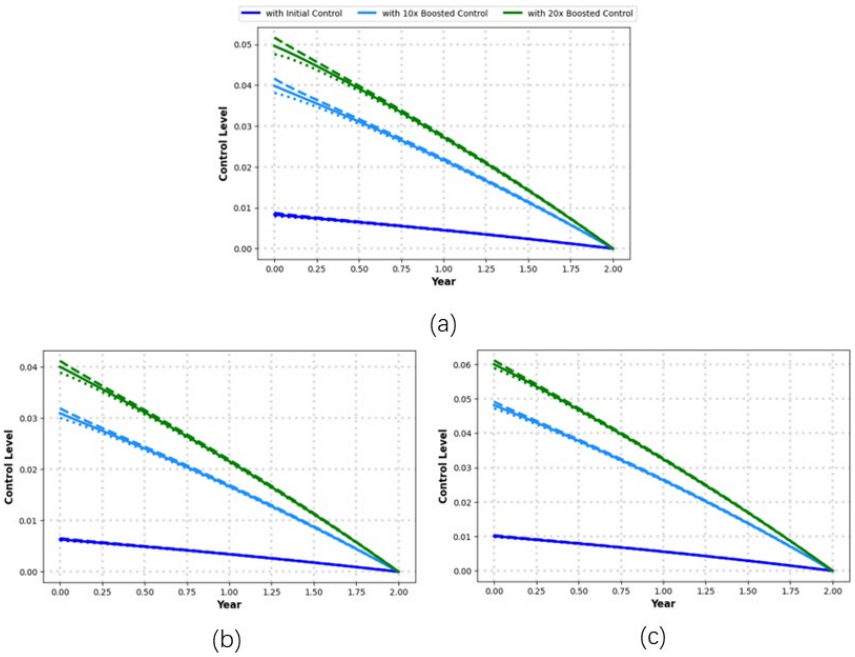

Figure 6. Control function graph of antibacterial usage (a) scenario II, (b) scenario V, and (c) scenario VI in condition II. Within each result, the solid line represents the baseline, while dotted and dashed lines correspond to a 5% decrease and increase in Λ_2, respectively.

7. Concluding remarks

In this study, we proposed a deterministic model for caries bacterial dynamics. We motivated ourselves with the developed models in [39] and [40]. The difference between the two models and our model is that we accommodated several dominant bacteria studied in many articles and considered the interactions and influences between the bacteria. Our proposed model of bacteria dynamics in oral biofilms are formulated. In this study, *S. sanguinis*, *S. mutans*, and *Veillonella spp.* along with their interactions were the modeling objects. The model was formulated by considering intervention efforts in the form of antibacterials to control each bacterium and reduce the risk of dental caries.

A dynamics analysis was conducted to gain insight into the existence of solutions and equilibrium solutions with their respective stabilities. The existence of the model solution represented by the results of the proofs in Theorem 1 and Lemma 2 was obtained using the method proposed in [54]. The model in system (1) had five equilibrium solutions, namely one trivial solution, 3 non-trivial solutions, and one interior solution. The interior solution represented the condition when all bacterial populations exist and

could survive in oral biofilms. The dynamic analysis results showed that the model solution could be interpreted as a biological element. The stability analysis of the trivial and non-trivial solutions 1– 3 used the Routh-Hurwitz stability criteria. Meanwhile, the stability of the interior solution was proven using a method similar to the method used by [57,58]. A sensitivity analysis revealed that the existence of *Veillonella spp.* was positively correlated with an increased risk of dental caries. This confirmed the results regarding the role of *Veillonella spp.* in the incidence of dental caries, as stated in [13,20].

The optimal control model was constructed by introducing a control variable that represented the frequency of antibacterial use. The solution of the constructed control model was determined by utilizing the Pontryagin maximum principle. The control simulation results showed that under condition II, the use of antibacterial scenario II produced the best solution compared to other scenarios. This meant that antibacterial scenario II was better at controlling the growth of the bacterial population of *S. mutans*, *S. sanguinis*, and *Veillonella spp.* in oral biofilms when condition II acted as a competition coefficient between *S. mutans* and *S. sanguinis*.

As revealed in [38], this study was the third deterministic model in the mathematical-dental scope to study the dynamics of bacteria in oral biofilm. The involvement of three bacteria was an advantage compared to both models in [39,40], which also left room for further development. For instance, to respond to the external factors that influenced bacterial dynamics in oral biofilms, the next study must consider the pH dynamics that affects each bacterium's survival rate. Consequently, the projection of caries risk could be reliable in real conditions, though this must be studied further.

Furthermore, a control effectiveness analysis could be explored by considering the Average Cost-Effectiveness Ratio (ACER) and the Incremental Cost-Effectiveness Ratio (ICER) on the optimal control results. In addition, Reinforcement Learning (RL) can be applied, where an intelligent agent learns an optimal policy through direct interaction under a dynamic environment. This approach, as previously used in [59,60], leads to a control policy that adapts in real-time to unpredictable changes in parameters, thus significantly enhancing its practicality. Utilizing such AI-driven methods with our foundational model could be a crucial next step in generating robust interventions against pathogenic biofilms. Nevertheless, this study was a breakthrough in expanding the deterministic mathematical study using an ODE system. In addition, this could be utilized to motivate and bridge the study between applied mathematics and dentistry to result in a more realistic model and reliable results to represent the real conditions.

Author contributions

Sanubari Tansah Tresna: Conceptualization, Methodology, Formal analysis, Investigation, Writing-original draft, Visualization; Nursanti Anggriani: Conceptualization, Methodology, Validation, Formal analysis, Investigation, Writing-review draft, Supervision, Funding acquisition; Herlina Napitupulu: Conceptualization, Methodology, Validation, Data curation, Writing-review draft, Supervision; Wan Muhamad Amir W. Ahmad: Conceptualization, Validation, Writing-review draft, Supervision. All authors have read and agreed to the published version of manuscript.

Use of Generative-AI tools declaration

The authors declare they have not used Artificial Intelligence (AI) tools in the creation of this article.

Acknowledgments

We are grateful to the associate editor and the reviewers for their comments and suggestions on improving the quality of this study. This research was funded by the Universitas Padjadjaran, Indonesia, via the Beasiswa Program Doktoral Padjadjaran, No. 958/UN6.3.1/PT00/2025.

Conflict of interest

The authors declare that they have no competing interests.

References

1. *Oral health*, WHO, 2023. Available from: https://www.who.int/news-room/fact-sheets/detail/oral-health.
2. M. A. Peres, L. M. D. Macpherson, R. J. Weyant, B. Daly, M. R. Mathur, S. Listl, et al., Oral disease: A global public health challenge, *Lancet*, **394** (2019), 249–260. https://doi.org/10.1016/S0140-6736(19)31146-8
3. W. Qiu, Y. Zhou, Z. Li, T. Huang, Y. Xiao, L. Cheng, et al., Application of antibiotics/antimicrobial agents on dental caries, *BioMed Res. Int.*, **2020** (2020), 5658212. https://doi.org/10.1155/2020/5658212
4. A. M. Martini, B. S. Moricz, L. J. Woods, B. D. Jones, Type IV pili of Streptococcus sanguinis contribute to pathogenesis in experimental infective endocarditis, *Microbiol. Spectr.*, **9** (2021), e01752-21. https://doi.org/10.1128/spectrum.01752-21
5. Z. Ling, H. Tao, *Dental caries and systemic diseases*, Berlin: Springer, 2016. https://doi.org/10.1007/978-3-662-47450-1_8
6. G. Aarabi, G. Thomalla, G. Heydecke, U. Seedorf, Chronic oral infection: An emerging risk factor of cerebral small vessel disease, *Oral Dis.*, **25** (2019), 710–719. https://doi.org/10.1111/odi.12912
7. A. M. Martini, B. S. Moricz, A. K. Ripperger, P. M. Tran, M. E. Sharp, A. N. Forsythe, et al., Association of novel Streptococcus sanguinis virulence factors with pathogenesis in a native valve infective endocarditis model, *Front. Microbiol.*, **11** (2020), 10. https://doi.org/10.3389/fmicb.2020.00010
8. P. D. Marsh, Dental plaque as a biofilm and a microbial community-Implications for health and disease, *BMC Oral Health*, **6** (2006), S14. https://doi.org/10.1186/1472-6831-6-S1-S14
9. N. B. Pitts, D. T. Zero, P. D. Marsh, K. Ekstrand, J. A. Weintraub, F. Ramos-Gomez, et al., Dental caries, *Nat. Rev. Dis. Primers*, **3** (2017), 17030. https://doi.org/10.1038/nrdp.2017.30
10. Y. Zhu, Y. Wang, S. Zhang, J. Li, X. Li, Y. Ying, et al., Association of polymicrobial interactions with dental caries development and prevention, *Front. Microbiol.*, **14** (2023), 1162380. https://doi.org/10.3389/fmicb.2023.1162380
11. I. Mashima, F. Nakazawa, The influence of oral Veillonella species on biofilms formed by Streptococcus species, *Anaerobe*, **28** (2014), 54–61. https://doi.org/10.1016/j.anaerobe.2014.05.003
12. W. H. Bowen, R. A. Burne, H. Wu, H. Koo, Oral biofilms: pathogens, matrix, and polymicrobial interactions in microenvironments, *Trends Microbiol.*, **26** (2018), 229–242. https://doi.org/10.1016/j.tim.2017.09.008

13. P. Zhou, D. Manoil, G. N. Belibasakis, G. A. Kotsakis, Veillonellae: beyond bridging species in oral biofilm ecology, *Front. Oral Heal.*, **2** (2021), 774115. https://doi.org/10.3389/froh.2021.774115
14. D. P. Wicaksono, J. Washio, Y. Abikoa, D. Hitomi, T. Nobuhiro, Nitrite production from nitrate and its link with lactate metabolism in oral veillonella spp, *Appl. Environ. Microbiol.*, **86** (2020), e01255-20. https://doi.org/10.1128/AEM.01255-20
15. T. Do, D. Devine, P. D. Marsh, Oral biofilms: Molecular analysis, challenges, and future prospects in dental diagnostics, *Clin. Cosmet. Investig. Dent.*, **5** (2013), 11–19. https://doi.org/10.2147/CCIDE.S31005
16. R. J. Kolenbrander, P. E.; Jakubovics, N. S. Chalmers, N. I.; Palmer, Human Oral multispecies biofilms: bacterial communities in health and disease, *Biofilm Mode Life Mech. Adapt.*, 2007, 175–190.
17. Y. Zhang, J. Fang, J. Yang, X. Gao, L. Dong, X. Zheng, et al., Streptococcus mutans-associated bacteria in dental plaque of severe early childhood caries, *J. Oral Microbiol.*, **14** (2022), 2046309. https://doi.org/10.1080/20002297.2022.2046309
18. P. M. Corby, J. Lyons-Weiler, W. A. Bretz, T. C. Hart, J. A. Aas, T. Boumenna, et al., Microbial risk indicators of early childhood caries, *J. Clin. Microbiol.*, **43** (2005), 5753–5759. https://doi.org/10.1128/JCM.43.11.5753-5759.2005
19. A. L. Melok, L. H. Lee, S. A. M. Yussof, T. Chu, Green tea polyphenol epigallocatechin-3-gallate-stearate inhibits the growth of streptococcus mutans: A promising new approach in caries prevention, *Dent. J.*, **6** (2018), 38. https://doi.org/10.3390/dj6030038
20. A. S. Setiawan, R. R. Darwita, S. Susilawati, D. A. Maharani, A. A. Djais, Risk factors for early childhood caries based on identification of Veillonella spp. Using RT-PCR, *Pesqui. Bras. Odontopediatria Clin. Integr.*, **20** (2020), 147. https://doi.org/10.1590/pboci.2020.147
21. K. Havsed, G. Hänsel Petersson, P. E. Isberg, M. Pigg, G. Svensäter, M. Rohlin, Multivariable prediction models of caries increment: a systematic review and critical appraisal, *Syst. Rev.*, **12** (2023), 202. https://doi.org/10.1186/s13643-023-02298-y
22. V. P. Mathur, J. K. Dhillon, Dental caries: a disease which needs attention, *Indian J. Pediatr.*, **85** (2018), 202–206. https://doi.org/10.1007/s12098-017-2381-6
23. S. Czajkowska, N. Potempa, J. Rupa-Matysek, A. Surdacka, Preventing the suspension of dental clinics by minimizing the risk of SARS-CoV-2 transmission during dental treatment, *Dent. Med. Probl.*, **58** (2021), 397–403. https://doi.org/10.17219/dmp/133442
24. G. Cherukuri, C. Veeramachaneni, G. V. Rao, V. B. Pacha, S. B. Balla, Insight into status of dental caries vaccination: A review, *J. Conserv. Dent.*, **23** (2020), 544–549. https://doi.org/10.4103/JCD.JCD_402_20
25. M. Patel, Dental caries vaccine: Are we there yet? *Lett. Appl. Microbiol.*, **70** (2020), 2–12. https://doi.org/10.1111/lam.13218
26. V. T. Sakai, T. M. Oliveira, T. C. Silva, A. B. S. Moretti, D. Geller-Palti, V. A. Biella, et al., Knowledge and attitude of parents or caretakers regarding transmissibility os caries disease, *J. Appl. Oral Sci.*, **16** (2008), 150–154. https://doi.org/10.1590/S1678-77572008000200013
27. X. Kuang, V. Chen, X. Xu, Novel approaches to the control of oral microbial biofilms, *Biomed Res. Int.*, **2018** (2018), 6498932. https://doi.org/10.1155/2018/6498932
28. E. T. Lofgren, M. E. Halloran, C. M. Rivers, J. M. Drake, T. C. Porco, B. Lewis, et al., Opinion: mathematical models: a key tool for outbreak response, *Proc. Natl. Acad. Sci. U. S. A.*, **111** (2014), 18095–18096. https://doi.org/10.1073/pnas.1421551111

29. B. D. Pandey, K. Pandeya, B. Neupane, Y. Shah, K. P. Adhikary, I. Gautam, et al., Persistent dengue emergence: The 7 years surrounding the 2010 epidemic in Nepal, *Trans. R. Soc. Trop. Med. Hyg.*, **109** (2015), 775–782. https://doi.org/10.1093/trstmh/trv087
30. D. Stanescu, B. M. Chen-Charpentier, Random coefficient differential equation models for bacterial growth, *Math. Comput. Model.*, **50** (2009), 885–895. https://doi.org/10.1016/j.mcm.2009.05.017
31. M. Scott, T. Hwa, Bacterial growth laws and their applications, *Curr. Opin. Biotechnol.*, **22** (2011), 559–565. https://doi.org/10.1016/j.copbio.2011.04.014
32. E. Ibargüen-Mondragón, S. Mosquera, M. Cerón, E. M. Burbano-Rosero, S. P. Hidalgo-Bonilla, L. Esteva, et al., Mathematical modeling on bacterial resistance to multiple antibiotics caused by spontaneous mutations, *Biosyst.*, **117** (2014), 60–67. https://doi.org/10.1016/j.biosystems.2014.01.005
33. N. G. Cogan, H. Rath, N. Kommerein, S. N. Stumpp, M. Stiesch, Theoretical and experimental evidence for eliminating persister bacteria by manipulating killing timing, *FEMS Microbiol. Lett.*, **363** (2016), 264. https://doi.org/10.1093/femsle/fnw264
34. C. Benjamín, P. Luis, C. L. Fernando, Modeling the effects of pH variation and bacteriocin synthesis on bacterial growth, *Appl. Math. Model.*, **110** (2022), 285–297. https://doi.org/10.1016/j.apm.2022.05.014
35. A. M. Smith, J. A. McCullers, F. R. Adler, Mathematical model of a three-stage innate immune response to a pneumococcal lung infection, *J. Theor. Biol.*, **276** (2011), 106–116. https://doi.org/10.1016/j.jtbi.2011.01.052
36. M. Cantone, G. Santos, P. Wentker, X. Lai, J. Vera, Multiplicity of mathematical modeling strategies to search for molecular and cellular insights into bacteria lung infection, *Front. Physiol.*, **8** (2017), 645. https://doi.org/10.3389/fphys.2017.00645
37. E. Domínguez-Hüttinger, N. J. Boon, T. B. Clarke, R. J. Tanaka, Mathematical modeling of Streptococcus pneumoniae colonization, invasive infection and treatment, *Front. Physiol.*, **8** (2017), 115. https://doi.org/10.3389/fphys.2017.00115
38. S. T. Tresna, N. Anggriani, H. Napitupulu, W. M. A. W. Ahmad, Deterministic modeling of the issue of dental caries and oral bacterial growth: A brief review, *Mathematics*, **12** (2024), 2218. https://doi.org/10.3390/math12142218
39. Y. Shen, J. Zhao, C. De La Fuente-Núñez, Z. Wang, R. E. W. Hancock, C. R. Roberts, et al., Experimental and theoretical investigation of multispecies oral biofilm resistance to chlorhexidine treatment, *Sci. Rep.*, **6** (2016), 27537. https://doi.org/10.1038/srep27537
40. X. Jing, X. Huang, M. Haapasalo, Y. Shen, Q. Wang, Modeling oral multispecies biofilm recovery after antibacterial treatment, *Sci. Rep.*, **9** (2019), 804. https://doi.org/10.1038/s41598-018-37170-w
41. X. Yang, R. Liu, J. Zhu, T. Luo, Y. Zhan, C. Li, et al., Evaluating the microbial aerosol generated by dental instruments: addressing new challenges for oral healthcare in the hospital infection, *BMC Oral Health*, **23** (2023), 409. https://doi.org/10.1186/s12903-023-03109-5
42. N. B. Pitts, S. Twetman, J. Fisher, P. D. Marsh, Understanding dental caries as a non-communicable disease, *Br. Dent. J.*, **231** (2021), 749–753. https://doi.org/10.1038/s41415-021-3775-4
43. A. M. Abram, M. M. Szewczyk, S. G. Park, S. S. Sam, H. B. Eldana, F. J. Koria, et al., A co-association of Streptococcus mutans and Veillonella parvula/dispar in root caries patients and in vitro biofilms, *Infect. Immun.*, **90** (2022), e00355-22. https://doi.org/10.1128/iai.00355-22

44. N. D. Teixeira, A. K. Almeida de Lima, T. Do, C. M. Stefani, Meta-analysis using NGS data: The Veillonella species in dental caries, *Front. Oral Heal.*, **2** (2021), 770917. https://doi.org/10.3389/froh.2021.770917
45. A. Villhauer, D. Lynch, J. Warren, D. Drake, Assessment of diversity and fidelity of transmission of streptococcus mutans genotypes in American Indian and Southeast Iowa mother-child dyads, *Front. Dent. Med.*, **3** (2022), 871185. https://doi.org/10.3389/fdmed.2022.871185
46. L. Y. Zheng, A. Itzek, Z. Y. Chen, J. Kreth, Oxygen dependent pyruvate oxidase expression and production in Streptococcus sanguinis, *Int. J. Oral Sci.*, **3** (2011), 82–89. https://doi.org/10.4248/IJOS11030
47. B. Zhu, L. C. Macleod, T. Kitten, P. Xu, Streptococcus sanguinis biofilm formation & interaction with oral pathogens, *Future Microbiol.*, **13** (2018), 915–932. https://doi.org/10.2217/fmb-2018-0043
48. G. J. Mount, W. R. Hume, H. C. Ngo, M. S. Wolff, *Preservation and restoration of tooth structure*, 3 Eds., New York: Wiley Blackwell, 2016.
49. J. A. Lemos, S. R. Palmer, L. Zeng, Z. T. Wen, J. K. Kajfasz, I. A. Freires, et al., The Biology of Streptococcus mutans, M*icrobiol. Spectr.*, **176** (2018), 139–148. https://doi.org/10.1128/microbiolspec.GPP3-0051-2018
50. W. Kondo, Significant correlations between the bulk of the desquamated epithelium, Lactobacillus, Streptococcus, and Veillonella counts of the human mouth, *Jpn. J. Microbiol.*, **6** (1962), 41–52. https://doi.org/10.1111/j.1348-0421.1962.tb00237.x
51. P. Zhou, X. Li, I. Huang, F. Qi, Veillonella catalase protects the growth of Fusobacterium nucleatum in microaerophilic and Streptococcus gordonii-resident environments, *Environ. Microbiol.*, **83** (2017), e01079-17. https://doi.org/10.1128/AEM.01079-17
52. H. T. Pramesti, Streptococcus sanguinis as an opportunistic bacteria in human oral cavity: Adherence, colonization, and invasion, *Padjadjaran J. Dent.*, **28** (2016), 13515. https://doi.org/10.24198/pjd.vol28no1.13515
53. B. Erick, M. Mayengo, Modelling the dynamics of Cassava Mosaic Disease with non-cassava host plants, *Informat. Med. Unlocked*, **33** (2022) 101086. https://doi.org/10.1016/j.imu.2022.101086
54. S. Daudi, L. Luboobi, M. Kgosimore, D. Kuznetsov, Modelling the control of the impact of Fall Armyworm (Spodoptera frugiperda) infestations on maize production, *Int. J. Differ. Equ.*, **2021** (2021), 8838089. https://doi.org/10.1155/2021/8838089
55. F. Forouzannia, A. B. Gumel, Mathematical analysis of an age-structured model for malaria transmission dynamics, *Math. Biosci.*, **247** (2014), 80–94. https://doi.org/10.1016/j.mbs.2013.10.011
56. S. Marino, I. B. Hogue, C. J. Ray, D. E. Kirschner, A methodology for performing global uncertainty and sensitivity analysis in systems biology, *J. Theor. Biol.*, **254** (2008), 178–196. https://doi.org/10.1016/j.jtbi.2008.04.011
57. R. Xu, Z. Wang, F. Zhang, Global stability and Hopf bifurcations of an SEIR epidemiological model with logistic growth and time delay, *Appl. Math. Comput.*, **269** (2015) 332–342. https://doi.org/10.1016/j.amc.2015.07.084
58. J. Roy, M. Banerjee, Global stability of a predator-prey model with generalist predator, *Appl. Math. Lett.*, **142** (2023), 108659. https://doi.org/10.1016/j.aml.2023.108659
59. H. Li, G. Liu, L. Xiong, Z. Liang, X. Zhong, Meta-reinforcement learning for controlling malware propagation in internet of Underwater Things, *IEEE Trans. Netw. Sci. Eng.*, 2025. https://doi.org/10.1109/TNSE.2025.3572050

60. S. Shen, L. Xie, Y. Zhang, G. Wu, H. Zhang, S. Yu, Joint differential game and double deep Q-Networks for suppressing malware spread in industrial internet of things, *IEEE Trans. Inf. Forensics Secur.*, **18** (2023), 5302–5315. https://doi.org/10.1109/TIFS.2023.3307956

Appendix

We consider the Lyapunov function given by

$$L(S,M,V)=\left(S-S^*-S^*\ln\frac{S}{S^*}\right)+\left(M-M^*-M^*\ln\frac{M}{M^*}\right)+\left(V-V^*-V^*\ln\frac{V}{V^*}\right).$$

We calculate the time derivative of the above function and obtain

$$\frac{dL}{dt}=\left(1-\frac{S^*}{S}\right)\frac{dS}{dt}+\left(1-\frac{M^*}{M}\right)\frac{dM}{dt}+\left(1-\frac{V^*}{V}\right)\frac{dV}{dt}.$$

Next, we explore the following calculation results first,

$$\begin{aligned}\frac{dL}{dt}=&\left(1-\frac{S^*}{S}\right)\left[\Lambda_1\left(1-\frac{S}{K_S}\right)S-\frac{\zeta}{1+\alpha_1V}MS-\eta S\right]\\&+\left(1-\frac{M^*}{M}\right)\left[\Lambda_2\left(1-\frac{M}{K_M}\right)M-\frac{\zeta}{1+\alpha_2V}SM-\eta M\right]\\&+\left(1-\frac{V^*}{V}\right)\left[\Lambda_3\frac{\rho(M+S)}{1+\rho(M+S)}V-\mu_3V-\eta V\right],\end{aligned}$$

$$\begin{aligned}\frac{dL}{dt}=&\left(\frac{S-S^*}{S}\right)S\left[\Lambda\left(1-\frac{S}{K_S}\right)-\frac{\zeta}{1+\alpha_1V}M-\eta\right]+\left(\frac{M-M^*}{M}\right)M\left[\Lambda_2\left(1-\frac{M}{K_M}\right)-\frac{\zeta}{1+\alpha_2V}S-\eta\right]\\&+\left(\frac{V-V^*}{V}\right)V\left[\Lambda_3\frac{\rho(M+S)}{1+\rho(M+S)}-\eta\right],\end{aligned}$$

$$\begin{aligned}\frac{dL}{dt}=&(S-S^*)\left[\Lambda\left(1-\frac{S}{K_S}\right)-\frac{\zeta}{1+\alpha_1V}M-\eta\right]+(M-M^*)\left[\Lambda_2\left(1-\frac{M}{K_M}\right)-\frac{\zeta}{1+\alpha_2V}S-\eta\right]\\&+(V-V^*)\left[\Lambda_3\frac{\rho(M+S)}{1+\rho(M+S)}-\eta\right].\end{aligned}$$

Note that

$$\begin{aligned}\frac{dS}{dt}=\Lambda_1\left(1-\frac{S}{K_S}\right)-\frac{\zeta}{1+\alpha_1V}M-\eta=0\rightarrow\Lambda_1-\eta=\Lambda_1\frac{S^*}{K_s}+\frac{\zeta}{1+\alpha_1V^*}M^*,\\\frac{dM}{dt}=\Lambda_2\left(1-\frac{M}{K_M}\right)-\frac{\zeta}{1+\alpha_2V}S-\eta=0\rightarrow\Lambda_2-\eta=\Lambda_2\frac{M^*}{K_m}+\frac{\zeta}{1+\alpha_2V^*}S^*,\\\frac{dV}{dt}=\Lambda_3\frac{\rho(M+S)}{1+\rho(M+S)}-\eta=0\rightarrow\eta=\Lambda_3\frac{\rho(S^*+M^*)}{1+\rho(S^*+M^*)}.\end{aligned}$$

Therefore, we obtain following results

$$\frac{dL}{dt} = (S - S^*)\left[\Lambda_1 \frac{S^*}{K_s} + \frac{\zeta}{1 + \alpha_1 V^*} M^* - \Lambda \frac{S}{K_s} - \frac{\zeta}{1 + \alpha_1 V} M\right]$$
$$+ (M - M^*)\left[\Lambda_2 \frac{M^*}{K_m} + \frac{\zeta}{1 + \alpha_2 V^*} S^* - \Lambda_2 \frac{M}{K_M} - \frac{\zeta}{1 + \alpha_2 V} S\right]$$
$$+ (V - V^*)\left[\Lambda_3 \frac{\rho(M + S)}{1 + \rho(M + S)} - \Lambda_3 \frac{\rho(S^* + M^*)}{1 + \rho(S^* + M^*)}\right],$$

$$\frac{dL}{dt} = (S - S^*)\left[\frac{\Lambda_1}{K_s}(S^* - S) + \frac{\zeta(M^* - M)}{1 + \alpha_1 V^*}\right] + (M - M^*)\left[\frac{\Lambda_2}{K_m}(M^* - M) + \frac{\zeta(S^* - S)}{1 + \alpha_2 V^*}\right]$$
$$+ (V - V^*)\left[\Lambda_3 \frac{\rho(M + S)}{1 + \rho(M + S)} - \Lambda_3 \frac{\rho(S^* + M^*)}{1 + \rho(S^* + M^*)}\right],$$

$$\frac{dL}{dt} = -\frac{\Lambda_1}{K_s}(S - S^*)^2 - \frac{\Lambda_2}{K_m}(M - M^*)^2 - \left[\frac{\zeta}{1 + \alpha_1 V^*} + \frac{\zeta}{1 + \alpha_2 V^*}\right](S - S^*)(M - M^*)$$
$$+ \Lambda_3\left[\frac{\rho(M + S)}{1 + \rho(M + S)} - \frac{\rho(S^* + M^*)}{1 + \rho(S^* + M^*)}\right](V - V^*).$$

Finally, we arrive at the result that can be used to ensure the global stability of the interior solution.